Biomimetic surface functionalization of clinically relevant metals used as orthopaedic and dental implants.

Biomimetic surface functionalization of clinically relevant metals used as orthopaedic and dental implants.

Elena García-Gareta[1,2], Jia Hua[1], Alodia Orera[3], Nupur Kohli[2], Jonathan C Knowles[4,5], Gordon W Blunn[1].

[1]John Scales Centre for Biomedical Engineering, Institute of Orthopaedics and Musculoskeletal Science, Division of Surgery and Interventional Science, University College London, Royal National Orthopaedic Hospital, Stanmore HA7 4LP, UK.

[2]Regenerative Biomaterials Group, RAFT Institute of Plastic Surgery, Mount Vernon Hospital, Northwood HA6 2RN, UK.

[3]Instituto de Ciencia de Materiales de Aragón (ICMA), CSIC and Universidad de Zaragoza, 50009 Zaragoza, Spain.

[4]Division of Biomaterials and Tissue Engineering, UCL Eastman Dental Institute, University College London, London WC1X 8LD, UK.

[5]Department of Nanobiomedical Science & BK21 Plus NBM Global Research Center for Regenerative Medicine, Dankook University, Cheonan 330-714, Republic of Korea.

Corresponding author:

Dr Elena García-Gareta

RAFT

Leopold Muller Building

Mount Vernon Hospital

Northwood HA6 2RN

United Kingdom

Tel: +44 1923 844555

Fax: +44 1923 844031

garciae@raft.ac.uk

Short Title: Biomimetic surface functionalization of metals.

Abstract

Titanium and its alloys or tantalum (Ta) are materials used in orthopaedic and dental implants due to their excellent mechanical properties and biocompatibility. However, their bioactivity and osteoconductivity is low. With a view to improving these materials bioactivity we hypothesised that the surface of Ta and TiAl6V4 can be functionalised with biomimetic, amorphous nano-sized calcium-phosphate (CaP) apatite-like deposits, instead of creating uniform coatings, which can lead to flaking, delamination and poor adherence. We used Ta and TiAl6V4 metal discs with smooth and rough surfaces. Amorphous CaP apatite-like particles were deposited on the different surfaces by a biomimetic rapid two-step soaking method using concentrated simulated body fluid (SBF) solutions without a pre-treatment of the metal surfaces to induce CaP deposition. Immersion times in the second SBF solution of 48 h and 18 h for Ta and TiAl6V4 respectively produced CaP deposits composed of amorphous globular nano-sized particles that also contained Mg, C and O. Longer immersion times produced more uniform coatings as well as an undesired calcite mineral phase. Prediction of *in vivo* behaviour by immersion in regular SBF showed that the obtained CaP deposits would act as a catalyst to rapidly form a Ca deficient CaP layer that also incorporates Mg. The amorphous CaP apatite-like deposits promoted initial attachment, proliferation and osteogenic differentiation of bone marrow derived mesenchymal stem cells. Finally, we used our method to functionalise 3D porous structures of titanium alloy made by selective laser sintering. Our study uses a novel and cost-effective approach to functionalise clinically relevant metal surfaces in order to increase the bioactivity of these materials, which could improve their clinical performance.

1. Introduction

Metals such as titanium (Ti) and its alloys or tantalum (Ta) are materials used in orthopaedic and dental implants due to their excellent mechanical properties and biocompatibility [1-4]. However, they present certain disadvantages with low bioactivity and poor osteoconductivity being notable ones [5]. Therefore, a significant amount of research is carried out to confer increased bioactivity to these materials. As surface properties of metal implants are critical features for rapid and stable integration with bone tissue the vast majority of this research focuses on surface modification and functionalization [5-7].

Surface topography modification has been extensively explored with studies showing that increasing surface roughness increases bone formation (osteoconduction) on the implant surface [8]. It has been shown both *in vitro* and *in vivo* that rough Ti surfaces promote osteogenic cell differentiation [8,9]. Moreover, a recent *in vitro* study by Hotchkiss and colleagues demonstrated the effect of Ti surface topography and wettability on macrophage activation and cytokine production [10]. Their results showed that macrophages cultured on rough, wettable metal surfaces produce an anti-inflammatory environment that may improve the healing response to implanted metal materials [10].

Another significant area of research is metal surface functionalization through deposition of a coating layer, commonly calcium phosphate (CaP) coatings due to their chemical similarity with bone mineral [1]. Apart from their excellent bioactivity, CaP materials and coatings are osteoconductive as they form a direct bond with bone tissue through formation of an apatite layer when implanted *in vivo* [11]. Another reason for the good osteointegration shown by CaP materials *in vivo* is that natural cytokines and adhesive proteins such as fibronectin adsorb to the surface of these materials providing a matrix for cell attachment [12,13]. However, the application of CaP coatings is limited by their relatively poor mechanical properties leading to flaking and delamination [14,15]. Another potential limitation of CaP coatings and materials is their composition. According to the current state of knowledge, bone mineral was recently described by Habraken and co-workers as "a poorly crystalline, highly substituted apatite consisting of very small crystals" [16]. The crystals in bone mineral are nanometer-sized platelets or needles that contain several ionic substitutions such as Mg^{2+}, Na^+ and Sr^{2+} in Ca^{2+} sites or CO_3^{2-} in OH^- (A-substitution) and PO_4^{3-} sites (B-substitution). In contrast, current CaP phases used for coatings i.e. hydroxyapatite [$Ca_{10}(PO_4)_6(OH)_2$ with Ca/P=1.67] or β-tricalcium phosphate [β-$Ca_3(PO_4)_2$ with Ca/P=1.50] lack the chemical variability of bone mineral. A current research trend is to produce

CaP materials that consist of precursor phases i.e. amorphous calcium phosphate [$Ca_3(PO4)_2 \cdot zH_2O$ where $z = 3$–4.5 in basic conditions and $M_3(Ca_3(HPO_4)_{4.5} \cdot zH_2O)$ where z is unknown and M is typically a monovalent cation (Na^+, K^+, NH_4^+) in acidic conditions; Ca/P=0.67-1.50] or octacalcium phosphate [$Ca_8H_2(PO_4)_6 \cdot 5H_2O$ with Ca/P=1.33] that can be rapidly converted to apatite after implantation [16].

For this study, we hypothesised that the surface of clinically relevant metals used in dental and orthopaedic implants can be functionalised with biomimetic, amorphous CaP apatite-like deposits. Our aim was to functionalise the metal surfaces with CaP deposits rather than creating uniform coatings, which can lead to flaking and delamination due to their relatively poor mechanical properties. Another aim of our work was to obtain CaP deposits composed of nano-particles, as the crystals in bone mineral are nano-sized. As both metals are widely used in dental and orthopaedic applications we used TiAl6V4 alloy and pure Ta metals, both with smooth and rough surfaces. Amorphous CaP apatite-like mineral particles were deposited on the different surfaces by a biomimetic soaking method using simulated body fluid (SBF) solutions without a pre-treatment of the metal surfaces to induce CaP deposition, thus offering an advantage in terms of simplicity and cost-effectiveness. As this method is not a line of sight coating then it can be used for treating the internal surfaces of porous alloys made by selective laser sintering. Prediction of *in vivo* behaviour was carried out by immersion in regular SBF. Finally, *in vitro* cell work using a clinically relevant source of cells (bone marrow derived mesenchymal stem cells, BM MSCs) was conducted to examine the biocompatibility and the osteogenic potential of the amorphous CaP deposits. Our study uses a novel and cost-effective approach to functionalise clinically relevant metal surfaces in order to increase the bioactivity of these materials, which could improve their clinical performance.

2. Materials and Methods

2.1 Materials

10 mm diameter × 2 mm thickness discs of pure Tantalum (Ta) and TiAl6V4 were used in this study (Fig. 1). Discs' surfaces were polished using silicon carbide grinding papers (Buehler, Germany) in a grinding machine (EXACT, Germany). Half of the discs were sandblasted using alumina particles (Al_2O_3) to obtain an average roughness of *Ra*=4.0 μm (Plasma Biotal Limited, UK). Samples were ultrasonically cleaned in acetone, 70% ethanol and distilled water for 15 minutes and air dried prior to the biomimetic soaking method. TiAl6V4 cubes

with 70% porosity were approximately 10 mm length, width and thickness (Eurocoating S.p.a, Ciré-Pergine, Italy), with 700-850 μm voids and 350-480 μm struts, fabricated using selective laser sintering (Fig. 1).

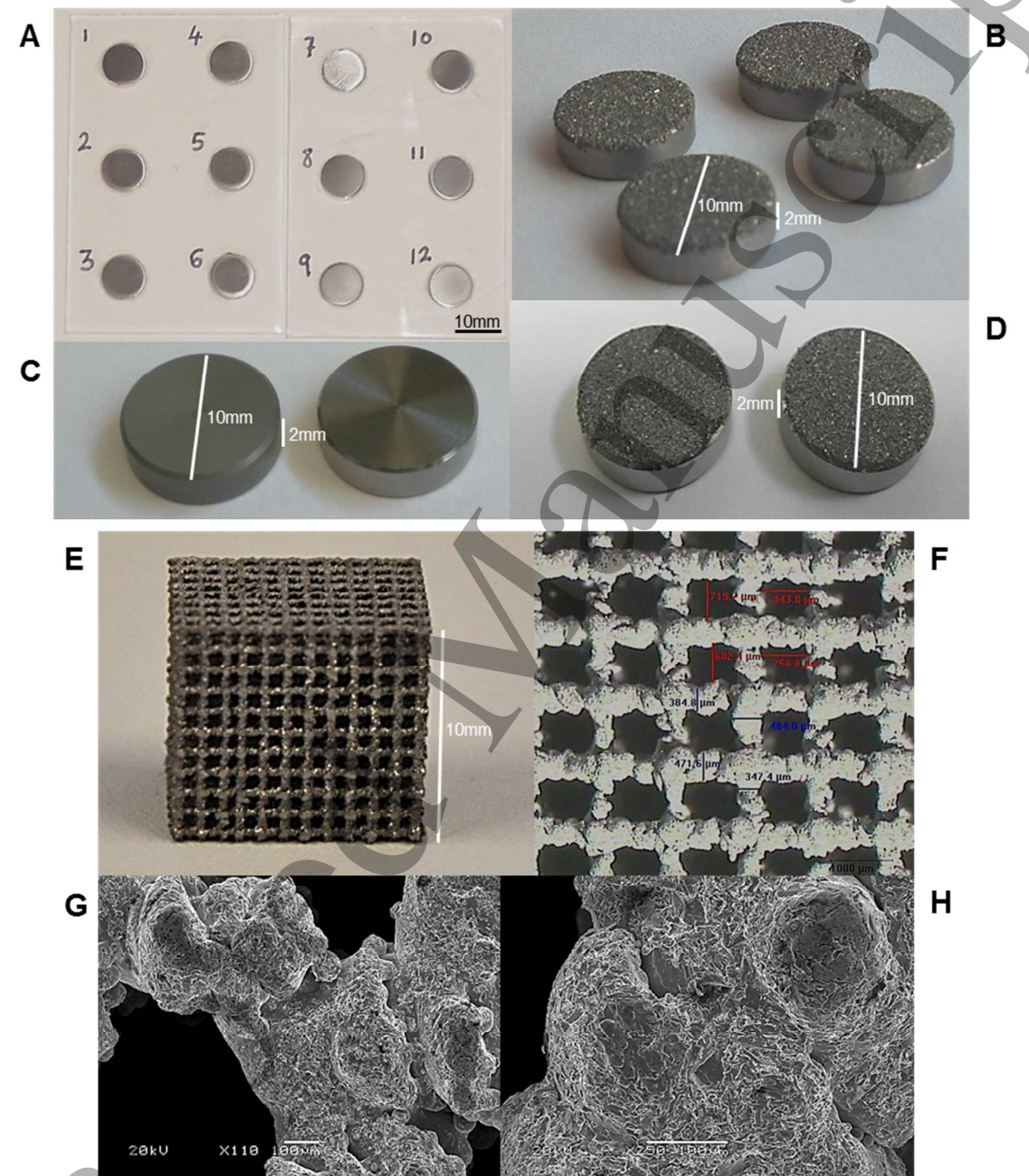**Figure 1.** Materials used in this study. A) Ta discs after being polished showing a smooth surface; B) sand-blasted Ta discs showing a rough surface; C) TiAl6V4 discs before being polished to obtain a smooth surface; D) sand-blasted TiAl6V4 discs showing a rough surface. Polished or rough Ta and TiAl6V4 discs had identical macroscopic appearance. E) Macroscopic image of porous TiAl6V4 cubes; F) microscopic view of the porous

TiAl6V4 material as supplied by the manufacturer; G and H) SEM images of the porous TiAl6V4 material revealing a rough surface.

2.2 Biomimetic soaking method

Table 1 shows the ion composition and concentration (mM) for both soaking solutions SBF-1 and SBF-2 as well as for regular SBF and human blood plasma (HBP). The appropriate quantities of reagent grade salts (NaCl, NaHCO$_3$, Na$_2$HPO$_4$, MgCl$_2$·6H$_2$O and CaCl$_2$·2H$_2$O; all BDH, UK) were dissolved in distilled water at 37ºC with a constant 5% CO$_2$ supply and stirring. Discs were firstly soaked in SBF-1, a solution 5 times more concentrated than regular SBF, for 24 h at 37ºC with constant vigorous stirring. Discs were soaked in SBF-2 solution, which has decreased concentrations of crystal growth inhibitors (Mg^{2+} and HCO$_3^-$), at 50ºC with constant stirring. In order to obtain amorphous CaP apatite-like crystals soaking time in SBF-2 was optimised first in Ta discs, which were soaked in SBF-2 for 48 h, 60 h or 72 h. Based on the results obtained for Ta discs, TiAl6V4 were soaked in SBF-2 for 18 h, 24 h or 48 h. Discs were not washed between the two soaking steps. Both steps were carried out in an incubator with 5% CO$_2$. The first step was carried out at 37ºC. For the second soaking step, the temperature was raised to 50ºC using a hot plate controlled with a thermometer. Finally, discs were cleaned in distilled water and air-dried for further analysis (Fig. 2).

Ion Concentration (mM)								
Solution	**Na$^+$**	**K$^+$**	**Ca^{2+}**	**Mg^{2+}**	**Cl$^-$**	**HPO$_4^{2-}$**	**HCO$_3^-$**	**SO$_4^{2-}$**
HBP	142.0	5.0	2.5	1.5	103.0	1.0	27.0	0.5
SBF	142.0	5.0	2.5	1.5	148.8	1.0	4.2	-
SBF-1	714.8	-	12.5	7.5	723.8	5.0	21.0	-
SBF-2	704.2	-	12.5	1.5	711.8	5.0	10.5	-

Table 1: Composition and concentration of ions present in human blood plasma (HBP), regular simulated body fluid (SBF) and soaking solutions SBF-1 and SBF-2.
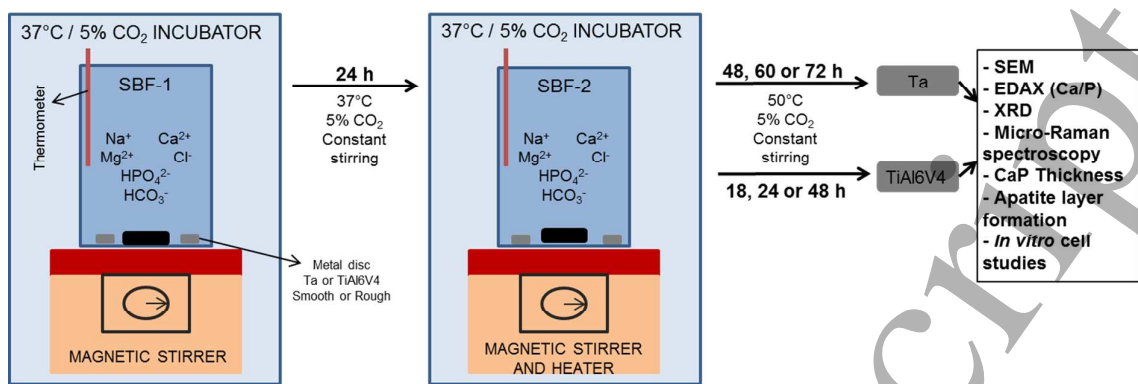
6

Figure 2. Diagram summarising the biomimetic soaking method used in this study.

2.3 Scanning electron microscopy (SEM) and energy dispersive X-ray spectroscopy (EDAX)

Morphology and size of mineral deposits were observed by SEM. Specimens were mounted on stubs and gold/palladium sputtered coated before observation under SEM (JEOL JSM 5500 LV). Elemental analysis was carried out by EDAX (EDAX Inc. USA). Calcium to Phosphorous (Ca/P) ratio was calculated from the quantitative data of the spectra (Atomic % Ca Kα / Atomic % P Kα).

2.4 X-ray diffraction (XRD)

Phase composition and crystallinity of the CaP deposits were studied by XRD using a Brüker D8 Advance Diffractometer (Brüker, UK) operated with Ni-filtered Cu Kα radiation and Brüker Lynx Eye detector. Data was collected from $2\theta = 10^\circ$ to 100° with a step size of 0.02° and a count time of 12 s per point.

2.5 Micro-Raman spectroscopy

Micro-Raman dispersion measurements were performed using a DILOR XY spectrometer with a CCD detector and a spectral resolution of 1.4 cm^{-1}. The 514.53 nm line of an Ar$^+$ ion laser was used as the excitation source and the scattered light was collected either through an X50 or X100 microscope objective lens.

2.6 Thickness of CaP deposits

Discs and porous 3D cubes were embedded in hard grade acrylic resin (LR White Resin, Agar Scientific), transversely cut using EXACT diamond band saw (EXACT, Germany) and polished using silicon carbide

7

grinding papers (Buehler, Germany) in a grinding machine (EXACT, Germany). Transversal sections were analysed by SEM.

2.7 Apatite layer formation

SBF (Table 1) was prepared using the appropriate quantities of reagent grade salts (NaCl, KCl, NaHCO$_3$, K$_2$HPO$_4$, MgCl$_2$·6H$_2$O and CaCl$_2$·2H$_2$O; all BDH, UK) dissolved in distilled water with constant stirring. The solution was buffered at pH 7.25 with (CH$_2$OH)$_3$CNH$_2$ 50mM/HCl 45mM buffer and kept at 37ºC. Discs were immersed for up to 7 days in SBF at 37ºC and surfaces analysed by SEM and EDAX at days 0, 1 and 7.

2.8 Culture and characterisation of ovine BM-MSCs

BM-MSCs were isolated from sheep bone marrow aspirates using Ficoll® gradients, expanded and maintained in tissue culture flasks. Dulbecco's modified eagles medium (Sigma-Aldrich, UK) with 10% fetal calf serum (First Link, UK) and 100 Units/mL of Penicillin/Streptomycin (Gibco, UK) (DMEM+) was used. Flasks were kept at 37ºC / 5%CO$_2$ and passaged when 80% confluent. BM-MSCs were differentiated down the adipogenic and osteogenic lineages to demonstrate their multipotency. For the adipogenic differentiation, 1×10^5 cells at P5 were seeded and cultured under either adipogenic (DMEM+ with 1μM dexamethasone, 200μM indomethacin, 500μM 1-methyl-3-isobutylxanthine and 10μg/mL Insulin; all from Sigma-Aldrich, UK) or standard conditions for 21 days on Thermanox™ discs placed at the bottom of the wells of a 12 well plate (Nalge Nunc International, USA). Media were changed every 3-5 days. After 21 days, presence of lipids was checked by Oil Red O staining. For the osteogenic differentiation, 3×10^4 cells at P5 were seeded and cultured under either osteogenic (DMEM+ with 0.1μM dexamethasone, 500μM ascorbic acid and 10mM β-glycerophosphate; all from Sigma-Aldrich, UK) or standard conditions up to 28 days on Thermanox™ discs. Media were changed every 3-5 days. Cell proliferation (DNA assay) and alkaline phosphatase (ALP) production per μg of DNA were analysed at days 7, 14, 21 and 28. Changes in cellular morphology were observed by phase-contrast light microscopy and SEM while mineral deposition was determined using Von Kossa staining at day 28.

2.9 Culture of BM-MSCs on metal discs

Discs were sterilised by autoclaving and seeded with BM-MSCs at P4 or P5. Each disc was seeded with 2.5x10^4 cells (2x10^4 for SEM) in a total volume of 50μL of DMEM+ onto the centre of the disc. After incubation for 100 minutes at 37ºC with 5%CO$_2$, 2-3mL of DMEM+ was added to each well. 12-well plates were kept in a

37ºC with 5%CO_2 incubator and media changed every 3-5 days. No osteogenic supplements were used. At days 4, 7 and 14 of culture, cell attachment (SEM), cell proliferation (alamarBlue® and DNA assays) and early osteogenic differentiation (ALP production per μg of DNA and cell morphology by SEM) were studied.

2.10 ALP activity and DNA assays

Cells were washed in phosphate buffer saline (PBS) and lysed by adding sterile distilled water at 37ºC. After being frozen at -70ºC and thawed 3 times, samples were spun at 10,000 rpm for 10 minutes. 50 μL of the supernatant were loaded into Cobas Bio® blue sample cups (AS Diagnostics, UK). Pre-weighed p-nitrophenol phosphate powder was mixed with 10mL of diethanolamine buffer (both Randox, UK) and pre-heated to 37 ºC to produce the working solution, which was loaded along with the samples into the Cobas Bio® analyser (Roche, UK). 250 μL of working solution were used for each sample. The ALP activity was calculated as U/L and normalised for the number of cells in the samples. 100 μL of the same supernatant used for the ALP production assay were loaded in triplicate for each sample into a FluoroNunc™ white 96-well plate. 100 μL of DNA (Sigma-Aldrich, UK) standards, ranging from 20 to 0.3125μg/mL, were loaded in triplicate. 100 μL of 1.0 μg/mL Hoechst 33258 dye (Sigma-Aldrich, UK) were added to each sample and fluorescence was read at 460 nm using a plate reader (Fluoroskan Ascent, Labsystems, USA). The amount of DNA in the samples was calculated as μg of DNA. ALP/DNA was expressed as U/μg.

2.11 alamarBlue® assay

3mL of 10% alamarBlue® (AbD Serotec, UK) diluted in phenol free DMEM (Sigma, UK) was added to the samples and an empty well (reference) and incubated at 37ºC with 5%CO_2 for 4 h. 100 μL from each sample was loaded in triplicate into a FluoroNunc™ white 96-well plate and fluorescence emission measured at 590 nm (Fluoroskan Ascent, Labsystems, USA).

2.12 Von Kossa staining

Cells were fixed in methanol, covered with 1.5% silver nitrate (Sigma, UK) and exposed to bright light for 1 h. The cells were washed with distilled water before covering with 2.5% sodium thiosulphate (BDH, UK) for 5 min. Finally, they were counterstained in Neutral Red (N6634, Sigma-Aldrich, UK) for 5 min, washed with distilled water, air dried and observed by light microscopy.

2.13 Oil Red O staining

0.5 g of Oil Red O (S267-2, Raymond A. Lamb, London, UK) was mixed with 100 mL of absolute isopropyl alcohol (296946H, BDH, UK) and left to stand overnight, while 1 g of dextrin (D2256, Sigma-Aldrich, UK) was added to 100 mL of distilled water. By mixing 60 mL of the Oil Red O stock solution with 40 mL of the dextrin stock solution an Oil Red O working solution was made and filtered before use with Whatman 540 filter paper. Cells were washed with PBS and fixed in formal saline. They were covered with Oil Red O stain for 20 minutes, rinsed with distilled water to remove excess stain and counter-stained with Harris Haematoxylin for 3 minutes. Finally, they were rinsed with distilled water, air-dried and observed under light microscopy.

2.14 SEM of cells on discs

Specimens were fixed in 2.5% glutaraldehyde (Agar Scientific, UK) overnight, washed with 0.1M sodium cacodylate buffer (Agar Scientific, UK) and post-fixed in 1% osmium tetroxide (Agar Scientific, UK) in 0.1M sodium cacodylate buffer for 1 h. After washing with 0.1M sodium cacodylate buffer, specimens were dehydrated through a graded series of industrial methylated spirit (20-60%) and ethanol (70-100%). Finally, they were treated for 2×4 minutes with hexamethyldisalazane (Agar Scientific, UK) and left to dry overnight. Specimens were mounted on stubs, gold/palladium sputtered coated and observed (JEOL JSM 5500 LV).

2.15 Statistical analysis

SPSS 14.0 software was used. Multiple comparisons were made using the Kruskal-Wallis test and comparisons between groups were made with Mann Whitney U test. A p-value≤0.05 was considered a significant result.

3. Results and Discussion

3.1 Biomimetic soaking method and characterisation of CaP deposits

Biomimetic soaking methods were originally developed by Kokubo *et al*. in the 1990s and are based on using SBFs that mimic physiological ionic strength and pH [17,18]. When materials are soaked in SBFs a thin apatite-like layer is obtained over time. Its main advantages are: i) the crystals obtained have been described as bone-like apatite crystals that are highly bioactive and resorbable; ii) it can be used to evenly coat complex 3D structures in contrast to the popular plasma spraying which is a line-of-sight method; iii) the process takes place at low temperatures (37 ºC - 50 ºC) and thus heat-sensitive materials such as polymers can be used, unlike other

coating methods such as plasma spraying that takes place at high temperatures thus limiting the range of materials that can be coated; and iv) since the process is carried out at low temperatures, biological molecules (i.e. growth factors) can be incorporated in the coating if desired. However, one disadvantage of the biomimetic method is that long immersion times (up to 30 days) in SBF are needed with daily refreshments of the solution due to its metastability [17]. Moreover, materials need to be pre-treated to induce precipitation of CaP crystals from SBF. In the case of metals, mixed-acid or alkali treatments are applied to roughen the metal surface to promote adhesion between CaP crystals and the substrate [19,20]. When working with Ti materials, researchers anodise their surface to create a TiO_2 layer that makes the surface more bioactive for the biomimetic soaking process [20]. Adding a pre-treatment step to the biomimetic soaking process introduces a layer of complexity to the procedure. In our study, no pre-treatment of samples was used to induce deposition of CaP deposits thus offering an advantage in terms of simplicity and cost-effectiveness.

The biomimetic soaking method used in this study was adapted from Habibovic *et al*. 2002, who used a rapid two step procedure on metal implants. Firstly, samples are soaked in a solution (SBF-1) that is five times more concentrated than regular simulated body fluid. In this first step the authors reported that a thin and uniform amorphous CaP layer was deposited on the metal surface. Secondly, samples are immersed in the SBF-2 solution, which has similar composition to that of SBF-1 but with decreased contents of crystal growth inhibitors (Mg^{2+} and HCO_3^-). During this second coating step, a fast precipitation of a 30 μm thick crystalline CaP coating was observed. The biomimetic coating produced by this two step procedure was found to closely resemble bone mineral [21]. Other rapid biomimetic procedures using concentrated SBF solutions can be found in the literature [22].

Our aim was to functionalise the metal surfaces with CaP apatite-like deposits rather than creating a uniform coating. We hypothesised that crystal growth can be controlled by controlling the immersion time in SBF-2.

3.1.1 Morphology and size of CaP deposits (SEM)

Our results showed that immersion time in SBF-2 influenced crystal morphology and growth (Fig. 3A). For Ta discs, 48 h of immersion in SBF-2 did not produce a uniform coating but rather deposits scattered through the surface. These deposits were amorphous nano-sized particles that aggregated to form globular structures in the micro-scale with nano-features such as nano-pores and nano-topography (Fig. 3A). An immersion time of 60 h

resulted in the formation of an amorphous coating that lacked a structure alongside the nano-sized deposits already seen together with plate-like crystals (Fig. 3A). SEM showed that the surface was entirely coated. Further immersion in SBF-2 (72 h) produced a uniform coating on the surface of the discs composed of mainly plate-like crystals in the micro-scale with a few of the nano-sized particles (Fig. 3A). For TiAl6V4 discs 48 h of immersion in SBF-2 resulted in the deposition of a uniform layer of plate-like crystals with some nano-sized particles (Fig. 3A). When immersion time in SBF-2 was reduced to 24 h similar results to 48h were seen. By further reducing the immersion time to 18 h only amorphous nano-sized particles organised in globular structures were observed (Fig. 3A). As in Ta, these globular deposits were found scattered over the surface. Surface topography (smooth or rough) was not found to affect particle morphology and growth. SEM analysis suggested that an immersion time of 48 h for Ta discs and 18 h for TiAl6V4 discs produced deposits composed of amorphous nano-sized particles.

3.1.2 Elemental composition (EDAX)

For both Ta and TiAl6V4 at the shortest times of immersion in SBF-2 (48 h and 18 h respectively) the deposits composed of amorphous nano-sized particles had Ca and P as main elements with Ca/P ratios below 1.67 (that of stoichiometric hydroxyapatite), suggesting they were Ca deficient (Fig. 3B). All the spectra contained carbon (C) and oxygen (O) peaks. Moreover, the majority of the spectra had a peak for Mg, one of the substituting elements found in bone mineral [23-25].

After 60 h and 24 h of immersion in SBF-2 for Ta and TiAl6V4 respectively a different crystal morphology developed (plate-like micro-crystals) suggesting the presence of a different mineral phase: EDAX showed that Ca and P were still the main elements but the Ca/P ratios were around 2, suggesting another mineral phase not as Ca deficient with considerably less P than the amorphous nano-sized particles (Fig. 3B). A Mg peak was still present in the majority of the spectra for both surfaces. At the longest times of incubation (72 h for Ta and 48 h for TiAl6V4) no P was detected in the EDAX spectra for coatings on Ta while for TiAl6V4 only one of the spectra showed a peak for P with a Ca/P=2.07 (Fig. 3B). This suggested that the other mineral phase present in the coatings was constituted primarily of Ca. It also suggested that with increasing immersion time in SBF-2 the Ca deficient CaP mineral phase of the nano-sized deposits converted into the Ca-rich mineral phase of the plate-like micro-crystals. This conversion was complete to a larger extent for Ta after 72 h immersion in SBF-2 than for TiAl6V4 after 48 h of immersion in SBF-2.
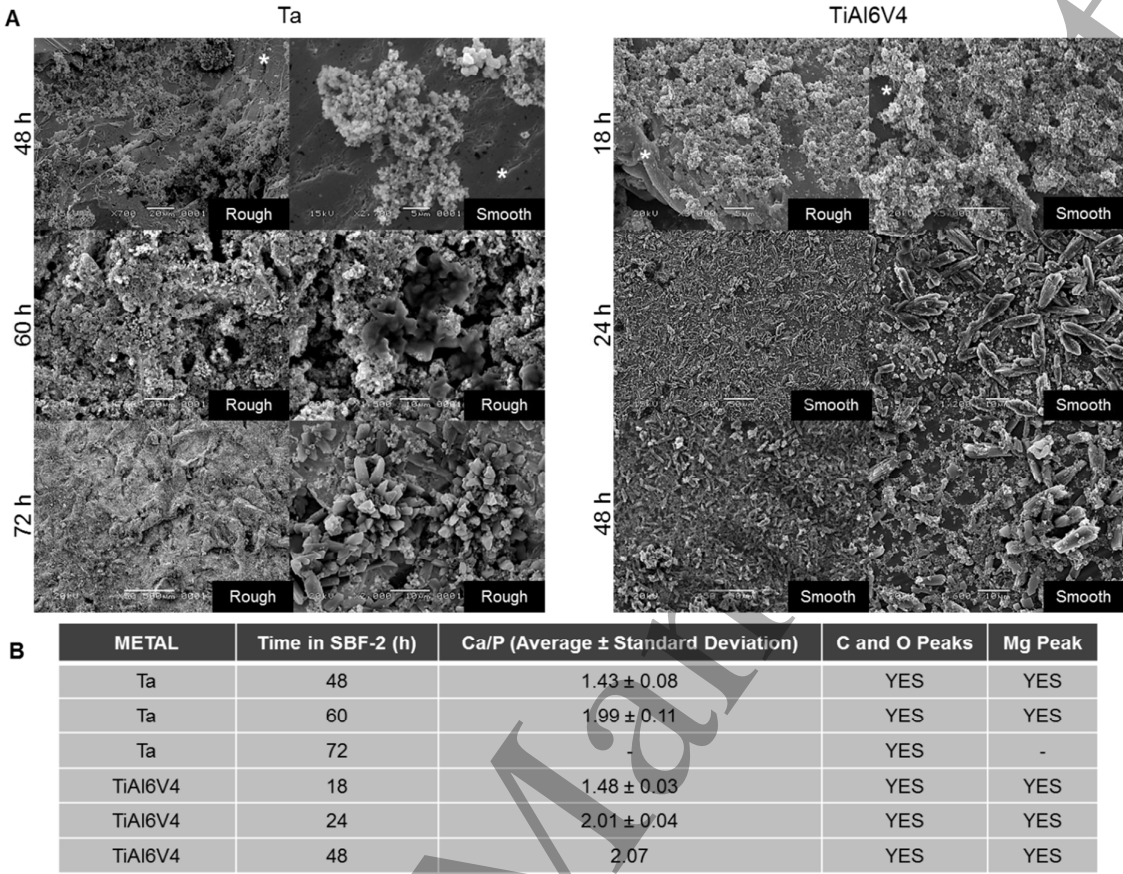
Figure 3. A) Representative SEM images for both Ta and TiAl6V4 showing the different mineral morphologies obtained with different immersion time in SBF-2. *shows uncoated metal disc surface. B) Summary of EDAX results.

3.1.3 Phase composition and crystallinity (XRD)

For the samples containing the CaP deposits composed of amorphous and nano-sized particles no peaks other than those corresponding to the metals were observed in the XRD patterns (Fig. 4). Amorphous phases composed of very small particles in the nano-metre scale usually give rise to very broad peaks or even an amorphous halo on XRD [26,27]. Samples containing both morphologies showed peaks corresponding to calcite ($CaCO_3$), a Ca mineral found in biological systems [28]. The peaks appeared large due to the very high symmetry for calcite.
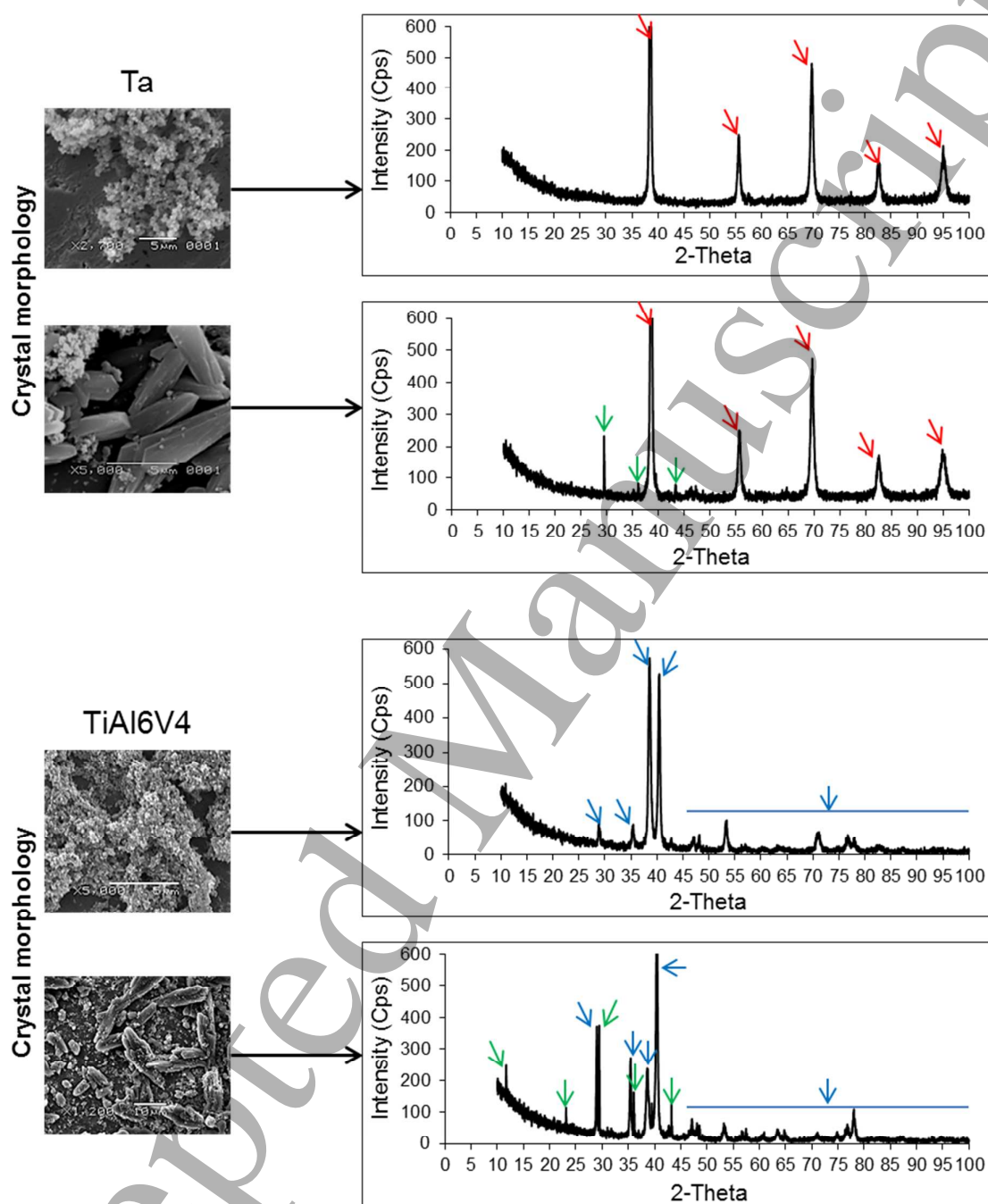
Figure 4. XRD results for both metals. Red arrows point at Ta peaks. Blue arrows point at TiAl6V4 peaks.

Green arrows point at peaks for calcite (CaCO₃).
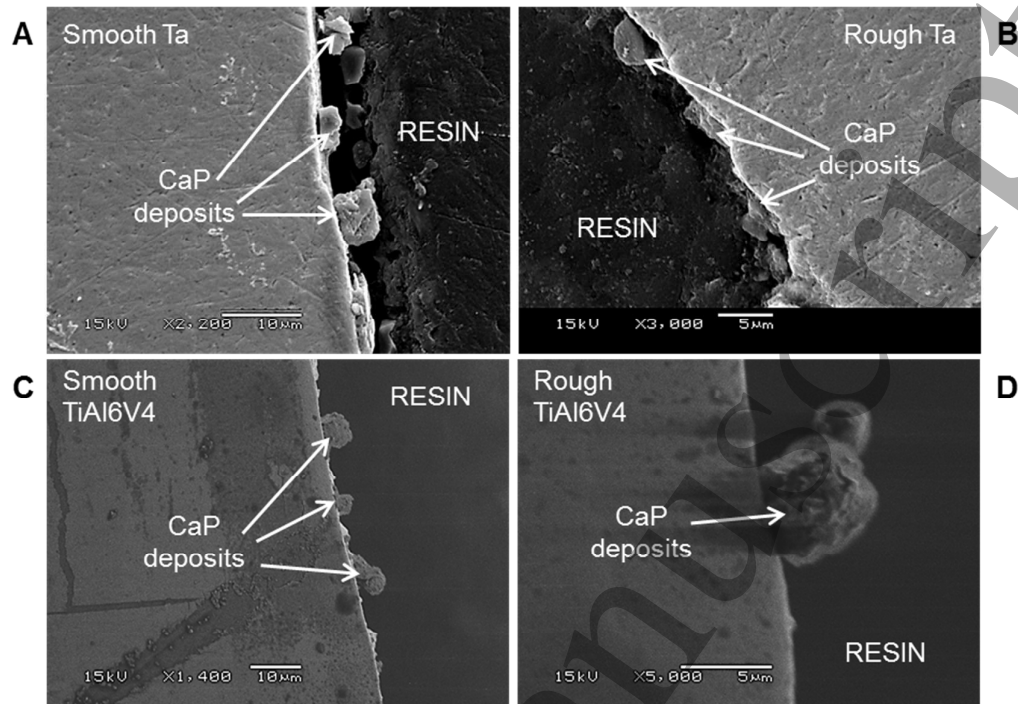
14

3.1.4 Micro-Raman spectroscopy

Smooth samples (both Ta and TiAl6V4) containing both morphologies showed bands at 154, 282, 711 and 1088 cm^{-1} corresponding to the calcite phase [29]. Both hydroxyapatite and β-tricalcium phosphate have phosphate groups that give an intense Raman band around 960 cm^{-1} (P-O symmetric stretch), so the absence of any band in that region indicated that no crystalline phosphate phases had been formed during the treatment.

All together, this data suggests that the biomimetic deposits are composed of an amorphous CaP phase, composed of nano-sized particles, which are Ca deficient. Mg, one of the reported substituting ions found in bone mineral [23-25], may be incorporated in the deposits. The presence of a C peak in the EDAX spectra could suggest the presence of a carbonate group in the deposits. However, it could also be due to general contamination as C is ubiquitous.

We concluded that 48 h and 18 h immersion time in SBF-2 for Ta and TiAl64 respectively were optimum. The difference in immersion time between both metals could be due to the excellent biocompatibility shown by titanium materials. The biocompatibility of these materials is based on a thin dioxide (TiO$_2$, in the case of titanium) layer formed on the surface of the bulk material. Ti is a very reactive element even at room temperature and a newly polished titanium surface will almost immediately have a thin layer of TiO$_2$ [1].

3.1.5 Thickness of CaP deposits

The maximum thickness of the CaP deposits after 48 h and 18 h immersion time in SBF-2 for Ta and TiAl64 respectively was determined by SEM (Fig. 5). Micrographs confirmed that the discs' surface was not completely covered by a mineral layer. The globular nature of the CaP deposits was also observed. Maximum thickness of the CaP deposits was slightly higher for TiAl6V4 than for Ta discs (Fig. 5).

Figure 5. Thickness of CaP deposits (SEM). A-D) Cross-sections of discs showing the globular CaP deposits scattered through the surfaces. E) Maximum thickness of CaP deposits as measured by SEM.

3.1.6 Apatite layer formation

As it has been shown that CaP materials promote direct bonding with bone tissue through formation of an apatite layer, *in vitro* models for studying apatite formation on the surface of different biomaterials are used as an assessment of their bioactivity and osteoconductivity. These *in vitro* models use the method developed by Kokubo and co-workers in the 1990s [17,18,30] where biomaterials are immersed in SBF and the mineral layer formed on their surface is subsequently characterised. Since surface topography and metal type did not affect the morphology and composition of CaP coatings deposited on TiAl6V4 and Ta discs, only TiAl6V4 discs with a smooth surface were used for this study. TiAl6V4 discs without CaP deposits were used as controls.

16

SEM analysis revealed mineral deposits at day 1 on control discs, which became denser after 7 days (Fig. 6A). Close observation of these deposits at day 1 showed that they were composed of 2 to 3μm diameter globular crystals that tended to aggregate in larger globular structures (Fig. 6A). These morphologies resemble the apatitic globular crystals described by Kokubo and co-workers on the surfaces of ceramics, metals and polymers when immersed in SBF [18,30]. Interestingly, at day 7 mineral deposits of nano-sized particles very similar to those observed after our biomimetic method, were seen (Fig. 6A, red arrows). Biomimetic CaP deposits became denser after immersion in SBF for 1 day and almost completely covered the disc surface (Fig. 6B). After 7 days, globular amorphous crystals in the micro-meter scale, were observed in some areas (Fig. 6B). Ca and P peaks were barely detected by EDAX analysis on the control discs at day 1 however, they were clearly visible at day 7, including a peak for Mg (Fig. 6A). For the discs with CaP deposits, apart from Ca, P, C and O peaks, Na, Cl and Mg peaks were also visible in the spectra. Calculated Ca/P ratios were similar to those observed at day 0 (Fig. 6B), showing that all the CaP deposits were Ca deficient.

These results suggest that the CaP deposits obtained following our biomimetic method would act as a catalyst to rapidly form a Ca deficient CaP layer that also incorporates Mg when incubated with SBF, thus demonstrating their bioactivity. Mg is one of the substituting ions in bone mineral [23] and recent research incorporating Mg into CaP materials and coatings have shown that it increases proliferation and osteogenic differentiation of both osteoprogenitor and osteoblast-like cells [31,32], as well as facilitating bone healing by providing immunomodulation and influencing crosstalk between macrophages and osteogenesis-related cells [32]. Furthermore, results also suggest that our biomimetic coating method accelerates the deposition mechanism of apatite crystals on metal surfaces normally observed after immersion in regular SBF: globular apatitic structures of 2-3 μm diameter are first deposited that later aggregate in larger globular structures, which then evolve into structures composed of CaP nano-sized crystals that incorporate available ions in the environment (i.e. Mg^{2+}).
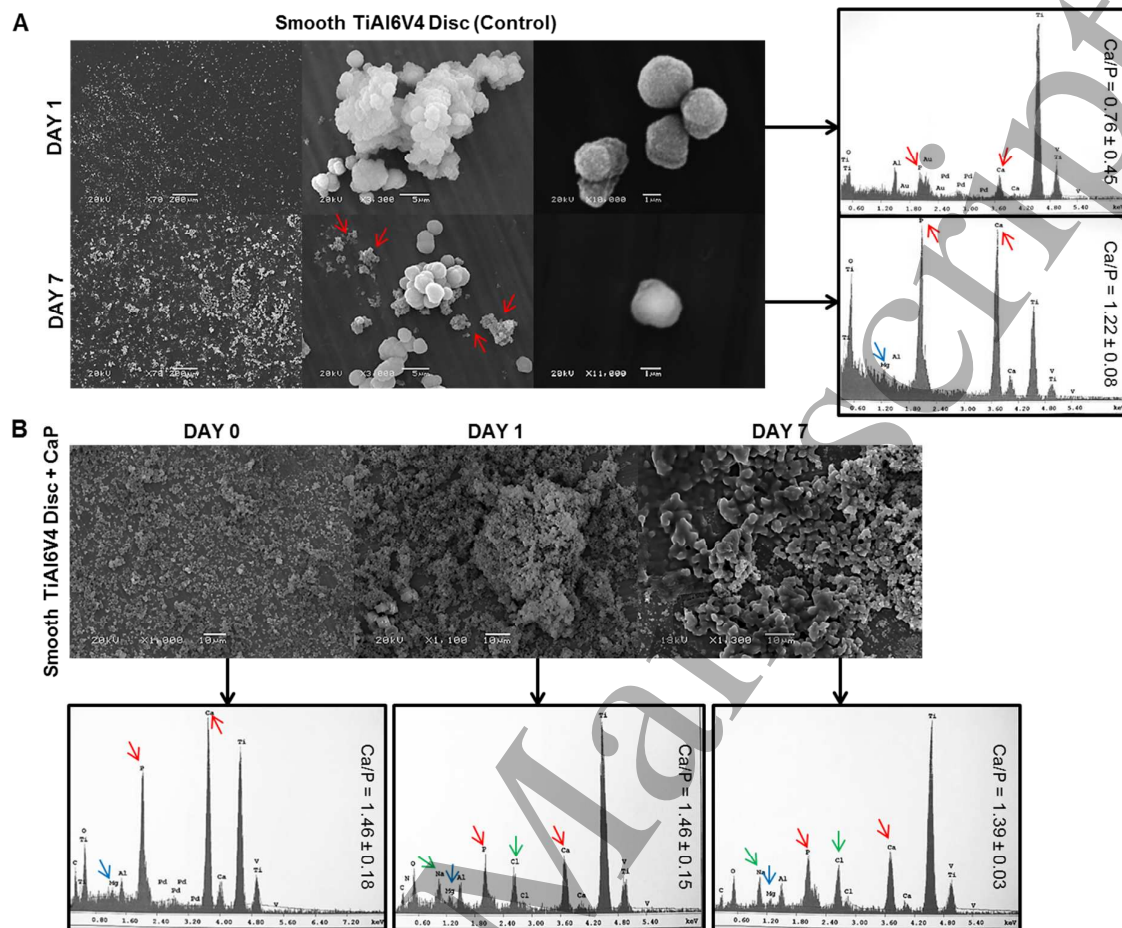
Figure 6. Apatite layer formation results. A) Smooth TiAl6V4 discs without CaP deposits (Control) and B) smooth TiAl6V4 discs with CaP deposits. Red arrows in SEM images point at mineral deposits of nano-sized particles. Red arrows in EDAX spectra point at Ca (main peak) and P peaks, blue arrows point at Mg peaks while green arrows point at Na and Cl peaks.

3.2 *In vitro* **cell work**

A clinically relevant source of cells was used to study biocompatibility and osteogenic potential of the CaP deposits. Following a bone injury, mesenchymal stem cells (MSCs) are recruited into the injury site and differentiate into bone cells due to environmental cues [34]. Moreover, MSCs secrete trophic agents and pro-angiogenic factors that recruit resident MSCs to the injury site and promote angiogenesis, which is critical for tissue regeneration [34].

3.2.1 Characterisation of BM-MSCs

Since the BM-MSCs used in this study were primary cells it was important to characterise them before seeding them on the materials. BM-MSCs were first described by Friedestein and co-workers in the 1970s, who observed that these cells adhered to tissue culture plates and resembled fibroblasts *in vitro* [35,36]. As BM-MSCs have the potential to differentiate into lineages of mesenchymal tissues, these cells are often characterised by demonstrating their multipotency differentiating them down two or more mesenchymal lineages [37-39], such as the adipogenic and osteogenic lineages. After 21 days of culture under adipogenic conditions, Oil Red O staining showed the presence of lipids as well as a clear difference in morphology (Fig. 7A) [37,38]. Changes in morphology were also observed in MSCs cultured under osteogenic conditions with cells becoming polygonal (Fig. 7B): an osteoblast feature [40]. Mineral deposits, representative of mineralised matrix formation, were stained with Von Kossa in the osteogenic samples after 28 days (Fig. 7B) [38]. DNA concentration (Fig. 7B) of BM-MSCs in osteogenic medium was higher at all time points than that of the control samples indicating that the osteogenic supplements added to the culture medium stimulated cell proliferation as well as differentiation [41,42]. ALP/DNA of osteogenic cultures was also higher at all time points, similar to that described in the literature (Fig. 7B) [41,43]. ALP activity elevates when BM-MSCs begin to differentiate and peaks between days 8 and 12 (day 14 in this study), which coincides with their commitment to become osteoblasts. Thus, ALP expression is an early marker of osteogenic differentiation. Together these results demonstrated the multipotency of the cells used in this study.
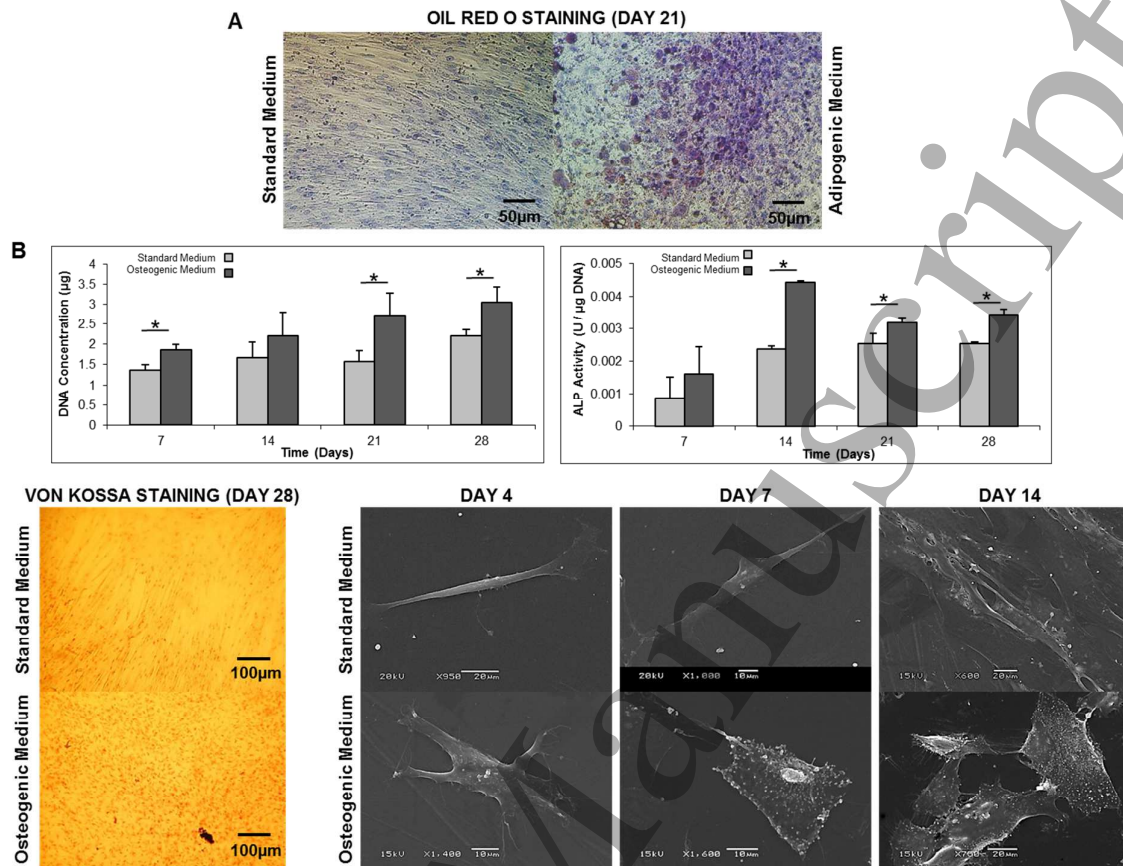
Figure 7. Characterisation of BM-MSCs. A) Adipogenic differentiation: Oil Red O staining at day 21 where red spots indicate presence of lipids. B) Osteogenic differentiation: DNA concentration and ALP/DNA activity (*p≤0.05), Von Kossa staining at ay 28 where black deposits indicate mineral deposition, SEM showing spindle-shaped cells in standard cultures and polygonal cells in osteogenic cultures.

3.2.2 Culture of BM-MSCs on metal discs

Since early implant fixation is the key to reduce the incidence of implant loosening [44,45], we investigated early (up to 14 days) BM-MSCs attachment, proliferation and osteogenic differentiation as an indication of initial cell response to the CaP deposits. Metal discs without CaP deposits were used as controls. No osteogenic supplements were used. Results showed that the CaP deposits increased initial attachment and proliferation of BM-MSCs (Fig. 8A,B). On the control discs cells proliferated more on smooth surfaces than on rough ones (Fig. 8A,B), as previously reported in an earlier study and in the literature [9,46]. This trend was also observed on the discs with CaP deposits although only at the early time points (days 4 and 7). In terms of early osteogenic differentiation, results showed that the CaP deposits induced osteogenic differentiation of BM-MSCs as

20

measured by ALP activity and was significantly higher on these surfaces compared to the controls (Fig. 8C). CaP materials and coatings have been shown to induce differentiation of MSCs down the osteogenic lineage [9,47,48] and we mentioned before that incorporating Mg into CaP materials has been shown to have a positive effect on proliferation and osteogenic differentiation of different cell types [31,32]. Therefore, our findings are consistent with previous reports and support the inclusion of Mg in CaP coatings for enhanced osteogenic differentiation of BM-MSCs. Furthermore, on the discs with CaP deposits, ALP activity was significantly higher on the rough surfaces than on the smooth ones on both days 7 and 14 (Fig. 8C). Finally, the type of metal (Ta or TiAl6V4) did not have a significant effect on early cell attachment, proliferation and differentiation.

SEM of control discs showed that on smooth surfaces cells were orientated to one another in a parallel way and displayed a flattened morphology. After 7 days in culture, cells were in contact with each other and displayed multiple cytoplasmic processes for cell attachment (Fig. 8D). On the other hand, patches of cells were observed covering the surface of rough discs (Fig. 8D). They were also in contact with each other and displayed long cytoplasmic processes. On the discs with CaP deposits, SEM at day 4 clearly showed that BM-MSCs use the CaP deposits to attach to the discs' surfaces. By day 7 a dense cell layer was seen covering the surface of the discs in some areas. By day 14 it was difficult of see individual cells as the discs' surfaces were almost confluent. Up to day 14 a mix of cellular shapes could be seen with two main morphologies distinguished: long, spindle cells and squarer, polygonal cells (Fig. 8D).

Together, these results suggest that the biomimetic, amorphous CaP apatite-like deposits promote initial attachment, proliferation and osteogenic differentiation of BM-MSCs.
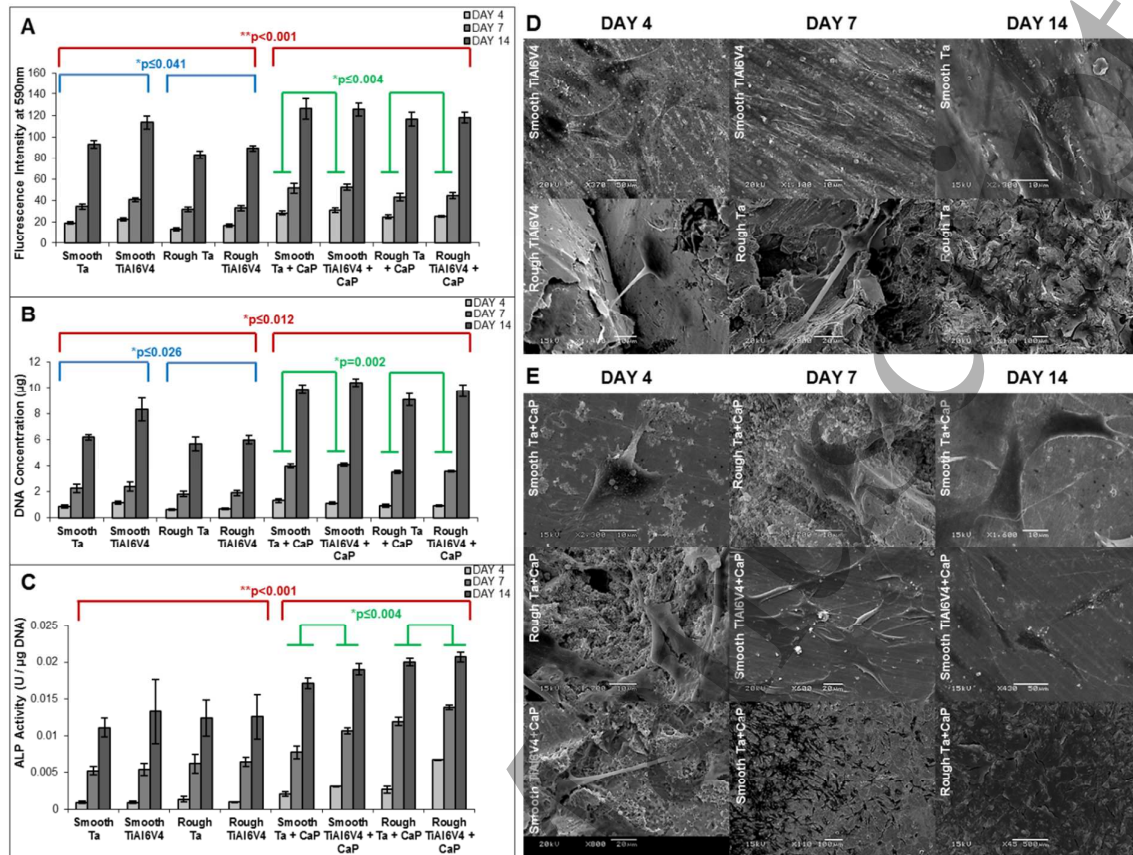
Figure 8. Culture of BM-MSCs on the metal discs for 14 days: A) alamarBlue activity assay; B) DNA concentration; C) ALP/DNA activity; D) SEM of control discs; and E) SEM of discs with CaP deposits.

3.3 3D porous structures

The last stage in our study was to use our method with selective laser sintered 3D porous metal structures, which are generating considerable interest due to their greater tissue ingrowth potential [1,45,49]. A highly porous structure that presents open and interconnected pores is advantageous: osteoblasts and MSCs migration and proliferation in the inner surfaces is necessary to form bone within the porous structures. A number of implants are now being made with porous surfaces. As plasma spraying hydroxyapatite is a line-of-site method, only the outer pores would be coated, so alternative methods for coating the inner porous surfaces are required such as solutions depositing CaP as outlined in this paper. In order for bone to penetrate deep into the porous structures vascularisation within the scaffold is necessary [50]. Moreover, 3D porous metal structures allow mechanical interlocking between the implant and host bone resulting in a greater stability of the implant. By controlling the porosity of the structure, a mismatch in elastic modulus between the implant and the host bone can be reduced,

22

thus minimising implant failure due to stress shielding [51]. In this study we used 3D porous TiAl6V4 structures and immersed them into in SBF-2 for 18 h as described previously for TiAl6V4 discs. Results showed that our method was able to deposit the amorphous nano-sized CaP particles already seen and described for TiAl6V4 discs throughout the 3D metal structure (Fig. 9).
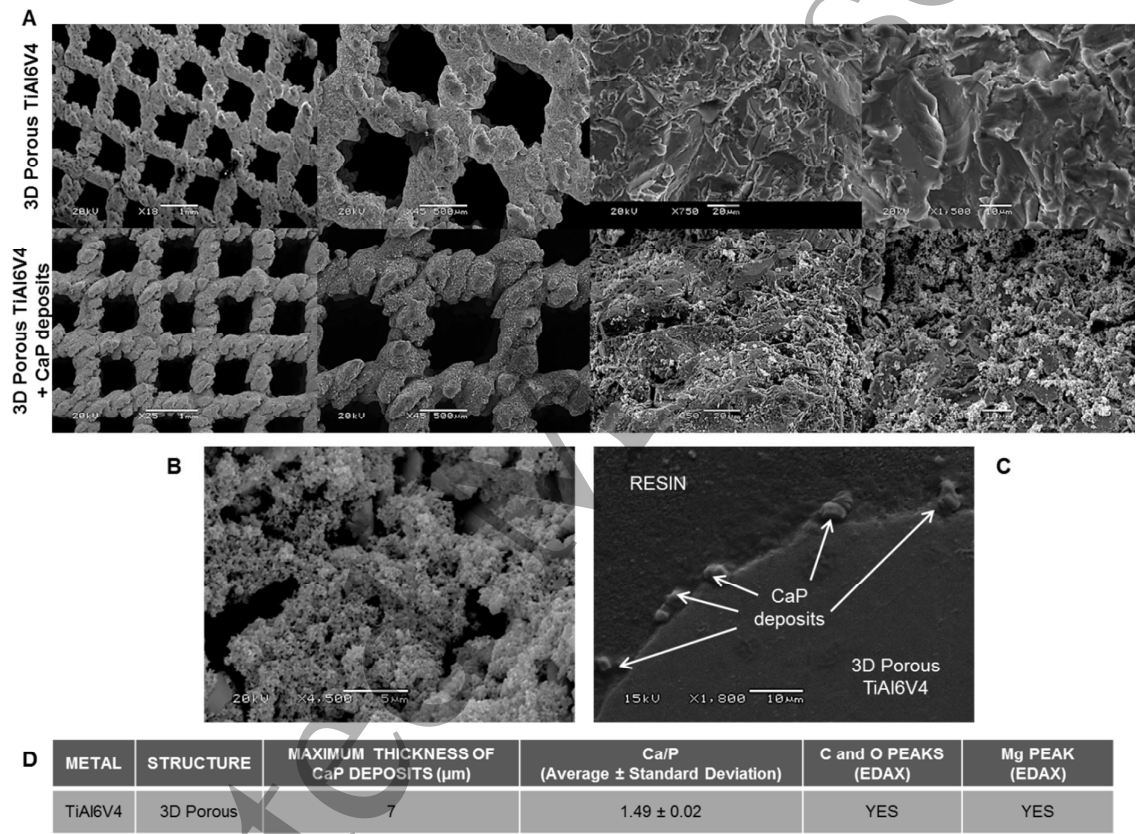

D	METAL	STRUCTURE	MAXIMUM THICKNESS OF CaP DEPOSITS (µm)	Ca/P (Average ± Standard Deviation)	C and O PEAKS (EDAX)	Mg PEAK (EDAX)
	TiAl6V4	3D Porous	7	1.49 ± 0.02	YES	YES

Figure 9. A) SEM comparison of 3D porous TiAl6V4 with and without CaP deposits. B) Representative SEM image of the amorphous nano-sized CaP particles deposited throughout the 3D porous TiAl6V4 structures. C) Cross-section of 3D porous TiAl6V4 showing CaP deposits inside the structure (SEM). D) Maximum thickness of CaP deposits as measured by SEM and summary of EDAX results.

23

4. Conclusions

We hypothesised that the surface of clinically relevant metals (Ta and TiAl6V4) used in dental and orthopaedic implants can be functionalised with biomimetic, amorphous CaP apatite-like deposits. Our aims were to functionalise the metal surfaces with CaP deposits instead of creating uniform coatings, and to obtain CaP deposits composed of nano-particles. Amorphous CaP particles were deposited on different surfaces by a biomimetic rapid two-step soaking method using concentrated SBF solutions without pre-treatment of the metal surfaces to induce CaP deposition. The CaP deposits were composed of amorphous globular nano-sized particles that also contained Mg, C and O. Immersion in regular SBF showed that the CaP deposits obtained following our biomimetic method would act as a catalyst to rapidly form a Ca deficient CaP layer that also incorporates Mg demonstrating their bioactivity. *In vitro* cell work showed that the amorphous CaP apatite-like deposits promote initial attachment, proliferation and osteogenic differentiation of BM-MSCs. Finally, our method could be applied to 3D structures in order to functionalise the inner porous surfaces .

The novelty of our work is the approach to functionalize metal surfaces with biomimetic CaP deposits (composed of nano-particles and include Mg) that would rapidly form a Ca deficient CaP layer that incorporates Mg upon implantation *in vivo*. Our data also shows that these CaP deposits would promote initial attachment, proliferation and osteogenic differentiation of BM-MSCs. So far, functionalization approaches focus on modifying metal surface topography or on producing thick CaP coatings. Our study is the first report that describes functionalisation of metal implants with bioactive, osteogenic and chemically versatile biomimetic CaP deposits. We believe that our approach has great potential for clinical translation and, due to the simplicity and cost-effectiveness of our method, it could be easily applicable in the coating prostheses industry.

References

[1] García-Gareta E, Coathup MJ, Blunn GW 2015. Osteoinduction of bone grafting materials for bone repair and regeneration. Bone 81:112-21.

[2] Peron C, Romanos G 2016. Immediate placement and occlusal loading of single-tooth restorations on partially threaded, titanium-tantalum combined dental implants: 1-year results. Int J Periodontics Restorative Cent 36(3):393-9.

[3] Romanos GE, Delgado-Ruiz RA, Sacks D, Calvo-Guirado JL 2016. Influence of the implant diameter and bone quality on the primary stability of porous tantalum trabecular metal dental implants: an in vitro biomechanical study. Clin Oral Implants Res doi:10.1111/clr.12792 [Epub ahead of print].

[4] Levine BR, Sporer S, Poggie RA, Della Valle CJ, Jacobs JJ 2006. Experimental and clinical performance of porous tantalum in orthopaedic surgery. Biomaterials 27:4671-81.

[5] Li J, Wu G, Jiang J, Zhao Y 2011. Surface characteristics and bioactivity of oxide films with haloid ions formed by micro-arc oxidation on titanium in vitro. Mater Manufacturing Processes 26(2):188-92.

[6] Salou L, Hoornaert A, Louarn G, Layrolle P 2015. Enhanced osseointegration of titanium implants with nanostructured surfaces: an experimental study in rabbits. Acta Biomater 11:494-502.

[7] Kohal RJ, Bächle M, Att W, Chaar S, Altmann B, Renz A, Butz F 2013. Osteoblast and bone tissue response to surface modified zirconia and titanium implant materials. Dent Mater 29(&):763-76.

[8] Du Z, Xiao Y, Hashimi S, Hamlet SM, Ivanovski S 2016. The effects of implant topography on osseointegration under estrogen deficiency induced osteoporotic conditions: Histomorphometric, transcriptional and ultrastructural analysis. Acta Biomater doi: 10.1016/j.actbio.2016.06.035 [Epub ahead of print].

[9] García-Gareta E, Hua J, Knowles JC, Blunn GW 2013. Comparison of mesenchymal stem cell proliferation and differentiation between biomimetic and electrochemical coatings on different topographic surfaces. J Mater Sci Mater Med 24(1):199-210.

[10] Hotchkiss KM, Reddy GB, Hyzy SL, Schawartz Z, Boyan BD, Olivares-Navarrete R 2016. Titanium surface characteristics, including topography and wettability, alter macrophage activation. Acta Biomater 31:425-34.

[11] Blokhuis TJ, Termaat MF, den Boer FC, Patka P, Bakker FC, Haarman HJThM 2000. Properties of calcium phosphate ceramics in relation to their in vivo behaviour. J Trauma Inj Inf Crit Care 48(1):179-186.

[12] Kilpadi KL, Chang P, Bellis SL 2001. Hydroxyapatite binds more serum proteins, purified integrins and osteoblast precursor cells than titanium or steel. J Biomed Mater Res 57:258-67.

[13] Hing KA 2005. Bioceramic bone graft substitutes: influence of porosity and chemistry. Int J Appl Ceram Technol 2(3):184-99.

[14] Toque JA, Herliansyah MK, Hamdi M, Ide-Ektessabi A, Sopyan I 2010. Adhesion failure behaviour of sputtered calcium phosphate thin film coatings evaluated using microscratch testing. J Mech Behav Biomed Mater 3(4):324-30.

[15] Reigstad O, Johansson C, Stenport V, Wennerberg A, Reigstad A, Rokkum M 2011. Different patterns of bone fixation with hydroxyapatite and resorbable CaP coatings in the rabbit tibia at 6, 12, and 52 weeks. J Biomed Mater Res B Appl Biomater 99(1):14-20.

[16] Habraken W, Habibovic P, Epple M, Bohner M 2016. Calcium phosphates in biomedical applications: materials for the future? Mater Today 19(2):69-87.

[17] Kokubo T, Kushitani H, Sakka S, Kitsugi T, Yamamuro T 1990. Solutions able to reproduce in vivo surface-structure changes in bioactive glass-ceramic A-W. J Biomed Mater Res 24:721-734.

[18] Kokubo T 1998. Apatite formation on surfaces of ceramics, metals and polymers in body environment. Acta Mater 46(7):2519-2527.

[19] Zhao JM, Park WU, Hwang KH, Lee JK, Yoon SY 2015. Biomimetic deposition of hydroxyapatite by mixed acid treatment of titanium surfaces. J Nanosci Nanotechnol 15(3):2552-5.

[20] Park IS, Yang EJ, Bae TS 2013. Effect of cyclic precalcification of nanotubular TiO2 layer on the bioactivity of titanium implant. Biomed Res Int ID 293627.

[21] Habibovic P, Barrère F, van Blitterswijk CA, de Groot K, Layrolle P 2002. Biomimetic hydroxyapatite coating on metal implants. J Am Ceram Soc 85(3):517-522.

[22] Liu Y, Wu G. de Groot K 2010. Biomimetic coatings for bone tissue engineering of critical-sized defects. *Journal of the Royal Society, Interface / the Royal Society*, 7 Suppl 5, pp.S631–47.

[23] Wopenka B, Pasteris JD 2005. A mineralogical perspective on the apatite in bone. Materials Science and Engineering C25:131-143.

[24] LeGeros RZ 1993. Biodegradation and bioresorption of calcium phosphate ceramics. Clinical Materials 14:65-88.

[25] LeGeros RZ 2008. Calcium phosphate-based osteoinductive materials. Chem Rev 108:4742-53.

[26] Suryanarayana X and Grant Norton M 1998. X ray diffraction: a practical approach. Plenum Press, New York.

[27] Hammond C 2001. The basics of crystallography and diffraction. Oxford University Press.

[28] Albeck S, Aizenberg J, Addadi L, Weiner S 1993. Interactions of various skeletal intracrystalline components with calcite crystals. J Am Chem Soc 115(25):11691-7.

[29] Gunasekaran S, Anbalagan G, Pandi S 2006. Raman and infrared spectra of carbonates of calcite structure. J Raman Spectrosc 37:892-9.

[30] Kokubo T, Kim HM, Kawashita M, Nakamura T 2001. Process of calcification on artificial materials. Z Kardiol 90(3):III/86-III/91.

[31] Park KD, Jung YS, Lee KK, Park HJ 2016. Behaviour of osteoblast-like cells on a β-tricalcium phosphate synthetic scaffold coated with calcium-phosphate and magnesium. J Craniofac Surg 27($):898-903.

[32] Singh SS, Roy A, Lee BE, Banerjee I, Kumta PN 2014. MC3T3-E1 proliferation and differentiation on biphasic mixtures of Mg substituted β-tricalcium phosphate and amorphous calcium phosphate. Mater Sci Eng C Mater Biol Appl 45:589-98.

[33] Wang M, Yu Y, Dai K, Ma Z, Liu Y, Wang J, Liu C 2016. Improved osteogenesis and angiogenesis of magnesium-doped calcium phosphate cement via macrophage immunomodulation. Biomater Sci 4(11):1574-83.

[34] Zigdon-Giladi H, Rudich U, Michaeli Geller G, Evron A 2015. Recent advances in bone regeneration using adult stem cells. World J Stem Cells 7(3):630-40.

[35] Friedenstein AJ, Chailakhjan RK, Lalykina KS 1970. The development of fibroblasts colonies in monolayer cultures of guinea-pig bone marrow and spleen cells. Cell Tissue Kinet 3, 393-403.

[36] Friedenstein AJ, Deriglasova UF, Kulagina NN, Panasuk AF, Rudakowa SF, Luriá EA, Ruadkow IA 1974. Precursors for fibroblasts in different populations of haematopoietic cells as detected by the in vitro colony assay method. Exp Hematol 2, 83-92.

[37] Pittenger MF, Mackay AM, Beck SC, Jaiswal RK, Douglas R, Mosca JD, Moorman MA, Simonetti DW, Craig S, Marshak DR 1999. Multilineage potential of adult human mesenchymal stem cells. Science 284:143-147.

[38] Erices A, Conget P, Minguell JJ 2000. Mesenchymal progenitor cells in human umbilical cord blood. British J Haematol 109:235-242.

[39] Hara M, Murakami T, Kobayashi E 2008. In vivo bioimaging using photogenic rats: fate of injected bone marrow-derived mesenchymal stromal cells. J Autoimmunity 30:163-171.

[40] Vrouwenvelder WCA, Groot CG, de Groot K 1993. Histological and biochemical evaluation of osteoblasts cultured on bioactive glass, hydroxylapatite, titanium alloy and stainless steel. J Biomed Mater Res 27:465-475.

[41] Jaiswal N, Haynesworth SE, Caplan AI, Bruder SP 1997. Osteogenic differentiation of purified, culture-expanded human mesenchymal stem cells in vitro. J Cell Biochem 64:295-312.

[42] Bruder SP, Jaiswal N, Haynesworth SE 1997. Growth kinetics, self-renewal and the osteogenic potential of purified human mesenchynal stem cells during extensive subcultivation and following cryopreservation. J Cell Biochem 64:278-294.

[43] Lian JB, Stein GS 1992. Concepts of osteoblast growth and differentiation: basis for modulation of bone cell development and tissue formation. Crit Rev Oral Biol Med 3(3):269-305.

[44] Ducheyne P, Beight J, Cuckler J, Evans B, Radin S 1990. Effect of calcium phosphate coating characteristics on early post-operative bone tissue ingrowth. Biomaterials 11, 531-540.

[45] Bobyn JD, Stackpool GJ, Hacking SA, Tanzer M, Krygier JJ 1999. Characteristics of bone ingrowth and interface mechanics of a new porous tantalum biomaterial. J Bone Joint Surg 81-B(5), 907-914.

[46] Anselme K, Bigerelle M, Noel B, Dufresne E, Judas D, Iost A, Hardouin P 2000. Qualitative and quantitative study of human osteoblast adhesion on materials with various surface roughnesses. J Biomed Mater Res 49(2):155-166.

[47] Ohgushi H, Dohi Y, Yoshikawa T, Tamai S, Tabata S, Okunaga K, Shibuya T 1996. Osteogenic differentiation of cultured marrow stromal stem cells on the surface of bioactive glass ceramics. J Biomed Mater Res 32:341-348.

[48] Nishio K, Neo M, Akiyama H, Nishiguchi S, Kim HM, Kokubo T, Nakamura T 2000. The effect of alkali- and heat-treated titanium and apatite-formed titanium on osteoblastic differentiation of bone marrow cells. J Biomed Mater Res 52(4):652-661.

[49] Loh QL, Choong C 2013. Three-dimensional scaffolds for tissue engineering applications: role of porosity and pore size. Tissue Eng Part B Rev 19(6):485-502.

[50] Karageorgiou V, Kaplan D 2005. Porosity of 3D biomaterial scaffolds and osteogenesis. Biomaterials 26:5474-91.

[51] Ryan G, Pandit A, Apatsidis DP 2006. Fabrication methods of porous metals for use in orthopaedic applications. Biomaterials 27:2651-2670.